RSC Advances

PAPER

View Article Online
View Journal | View Issue

Cite this: *RSC Adv.*, 2025, **15**, 35892

Observation of spin-crossover behaviour in Co(II)-terpyridine complexes possessing π-conjugated substations

Keita Soejima,†[a] Yoshihiro Sekine,†[abc] Kanta Miyake,[a] Kota Kiba,[a] Yuito Yamaguchi,[a] Hikaru Zenno[a] and Shinya Hayami*[ade]

Received 9th December 2024
Accepted 14th September 2025

DOI: 10.1039/d4ra08657k

rsc.li/rsc-advances

Exploring new compounds that exhibit spin-state switching under external stimuli is crucial for advancing materials science. However, the feasibility of combining π-conjugated moieties with Co(II)-terpy cation units *via* an ethynyl group has not yet been investigated. This approach represents a hybridization strategy wherein distinct functional moieties are incorporated into a single coordination metal complex to achieve multifunctionality. In this study, we synthesised a series of Co(II)-terpyridine complexes [Co(R-ethynyl-terpy)$_2$](BF$_4$)$_2$ (R = phenyl for **1**, naphthyl for **2**, anthracenyl for **3**, and pyrenyl for **4**), resolved their crystal structures and packing arrangements, and evaluated their magnetic properties using a superconducting quantum interference device magnetometer. These Co(II)-based complexes exhibited thermal spin-crossover behaviour in the solid state. Although complexes **1–4** were luminescent in solution, only complexes **3** and **4** emitted dual monomer and excimer fluorescence in solution due to their substituted π-conjugated moieties. Our findings are expected to serve as a platform for the synthesis of magnetically functional coordination metal compounds based on Co(II) ions for the potential development of photophysical materials.

1 Introduction

Designing functional materials based on coordination metal complexes that are responsive to external stimuli is important for the advancement of materials science.[1–5] Coordination complexes, for which the magnetic properties are switchable by external stimuli, including spin crossover (SCO) and valence tautomeric electron transfers,[6–19] are promising candidates for application in future molecular sensors or memory devices.

The SCO phenomenon, which entails transitioning between the low-spin (LS) and high-spin (HS) states, has been observed for coordination metal complexes with d^n (n = 4–7) transition metal ions.[8–10] In particular, Fe(II)-based SCO compounds have been extensively studied due to the notable changes in the magnetic properties between the LS Fe(II) (S = 0) and HS Fe(II) (S = 2) states. Conversely, Co(II) SCO complexes, which switch between their LS Co(II) (S = 1/2) and HS Co(II) (S = 3/2) states, are less well-known than their Fe(II) counterparts.[9,10] Consequently, new Co(II)-based materials that exhibit SCO behaviour are worthy of developing.

Previously, the development of Co(II) SCO complexes by our group and that of Murray, independently from one another, involved the syntheses of a series of Co(II) compounds with bis-terpyridine frameworks as ligands.[20] These frameworks are particularly attractive owing to the ease of chemical modification and appropriate ligand field strength for SCO in terpyridine skeletons, thus enabling the syntheses several Co(II)-based SCO complexes using terpyridine and derivatives thereof. For example, Co(II)-terpyridine complexes with long alkyl chains at position "4" exhibit unique SCO behaviour,[21] with the LS and HS Co(II) states stabilising at higher and lower temperatures, respectively, due to their flexible molecular dynamics. This phase transition is attributed to the complexes engaging in suitable intermolecular interactions in response to external stimuli. Apart from this, the introduction of π-conjugated substitution at the terpyridine unit can influence the spin-state-switching behaviour *via* various molecular packing structures. Our group reported that mononuclear Co complexes with π-conjugated substitution, specifically [Co(Naph-C2-terpy)$_2$](BF$_4$)$_2$ (Naph-C2-terpy = 4′-(2-naphthoxy(ethoxy))-2,2′ : 6′,2″-terpyridine), exhibit abrupt spin transitions.[22] The incorporation of π-conjugated moieties in coordination metal complexes affects

[a]*Department of Chemistry, Graduate School of Science and Technology, Kumamoto University, 2-39-1 Kurokami, Chuo-ku, Kumamoto 860-8555, Japan. E-mail: hayami@kumamoto-u.ac.jp*

[b]*Priority Organization for Innovation and Excellence, Kumamoto University, 2-39-1 Kurokami, Chuo-ku, Kumamoto 860-8555, Japan*

[c]*International Research Organization for Advanced Science and Technology, Kumamoto University, 2-39-1 Kurokami, Chuo-ku, Kumamoto 860-8555, Japan*

[d]*Institute of Industrial Nanomaterials (IINa), Kumamoto University, 2-39-1 Kurokami, Chuo-ku, Kumamoto 860-8555, Japan*

[e]*International Research Center for Agricultural and Environmental Biology (IRCAEB), Kumamoto University, 2-39-1 Kuro-kami, Chuo-ku, Kumamoto 860-8555, Japan*

† These authors contributed equally to this work.

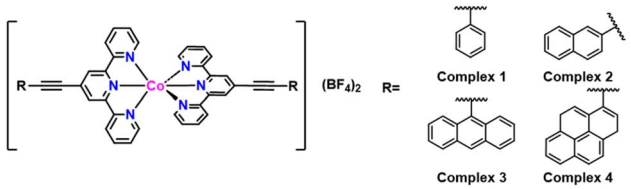

Scheme 1 Molecular structures of the Co(II)-complexes synthesised in this study.

their photophysical properties, thereby rendering these complexes potentially suitable for multifunctional molecular materials. However, the combination of π-conjugated moieties with Co(II)-terpy cationic units *via* an ethynyl group has not yet been reported.

Herein, we report the syntheses and physical properties of a new series of Co(II)-based terpyridine complexes possessing π-conjugated moieties through the ethynyl group. The terpyridine ligand derivatives of 4′-phenylethynyl-2,2′ : 6′,2″-terpyridine (ph-ethyl-terpy), 4′-(2-ethynyl-naphthalene)-2,2′ : 6′,2″-terpyridine (Naph-ethynyl-terpy), 4′-(9-ethynyl-anthracene)-2,2′ : 6′,2″-terpyridine (Ant-ethynyl-terpy), and 4″-(1-ethynyl-pyrene)-2,2″ : 6″,2‴-terpyridine (pyr-ethynyl-terpy) are utilised for the complexation of Co(II) ions to yield complexes **1–4**, respectively (Scheme 1).

2 Experimental methods

2.1 Preparation and characterisation of Co(II) complexes

All the chemicals were purchased from commercial sources and used without further purification. 4'-[[(Trifluoromethyl) sulfonyl]oxy]-2,2' : 6′,2″-terpyridine (OTf-terpy), ph-ethyl-terpy, and pyr-ethynyl-terpy[23–27] were prepared according to previously reported methods.

2.1.1 Synthesis of Nap-ethynyl-terpy. 9-Ethynylanthracene (390 mg, 2.74 mmol), OTf-terpy, and $[Pd(PPh_3)_4]$ (184 mg, 0.16 mmol) were dried under high vacuum (HV) in a two-neck flask. Ar-purged triethylamine (10 mL) and toluene (40 mL) were added, and argon was bubbled through the mixture for 30 min. Subsequently, the reaction mixture was stirred and heated at 130 °C for 24 h, after which the solvent was evaporated by placing the solution under HV. The crude product was chromatographed on alumina and eluted with a gradient of ethyl acetate in hexane from 0 to 50%. The product was analytically pure (326 mg, 27%). ^{1}H-NMR ($CDCl_3$): 8.78 (s, 4H), 8.73 (d, 2H), 8.69 (d, 2H), 8.50 (s, 1H), 8.037 (d, 2H), 7.91 (t, 2H), 7.67 (t, 2H), 7.56 (t, 2H), 7.38 (t, 2H). ^{13}C-NMR ($CDCl_3$): δ 155.9 (2C), 155.7 (2C), 149.4 (2C), 137.1 (2C), 133.6, 133.3, 133.1, 132.4, 128.5, 128.3, 128.1, 128.0, 127.2, 126.8, 124.2 (2C), 123.0 (2C), 121.4 (2C), 119.9, 94.3, 88.0.

2.1.2 Synthesis of Ant-ethynyl-terpy. 2-Ethynylnaphthalene (362 mg, 2.42 mmol), OTf-terpy, and $[Pd(PPh_3)_4]$ (167 mg, 0.15 mmol) were dried under HV in a two-neck flask. Ar-purged triethylamine (5 mL) and toluene (20 mL) were added, and argon was bubbled through the mixture for 30 min. Subsequently, the reaction mixture was stirred and heated at 130 °C for 24 h, after which the solvent was evaporated under vacuum. The crude product was chromatographed on alumina and eluted with a gradient of ethyl acetate in hexane from 0 to 50%. An analytically pure compound was obtained (673 mg, 73%). ^{1}H-NMR ($CDCl_3$): 8.107 (s, 1H), 7.89–7.83 (m, 6H), 7.66 (q, 1H), 7.60 (d, 1H), 7.54–7.45 (m, 4H), 7.36 (m, 2H).

2.1.3 Synthesis of $[Co(Ph\text{-}ethynyl\text{-}terpy)_2](BF_4)_2\cdot H_2O\cdot 0.5MeOH$ (1). Ph-ethynyl-terpy (0.080 g, 0.24 mmol) was dissolved in CH_3Cl (10 mL), and $Co(BF_4)_2\cdot 6H_2O$ (0.041 g, 0.12 mmol) dissolved in MeOH (10 mL) was added to the solution. The colour immediately changed to brown, and the solution was stirred for 3 h. Subsequently, it was concentrated, and the resulting precipitate was filtered to obtain a crude brown powder, which was then dissolved in MeOH and the solvent was evaporated slowly to obtain single crystals of **1**. Yield: 58%. Elemental analysis (%): calcd. for $C_{93}H_{68}B_4Co_2F_{16}N_{12}O_3$: calcd., C, 59.84; H, 3.67; N, 9.00. Found: C, 59.48; H, 3.79; N, 9.11. ESI-MS: calculated $m/z = 362.5932$, observed $m/z = 362.7989$.

2.1.4 Synthesis of $[Co(Naph\text{-}ethynyl\text{-}terpy)_2](BF_4)_2\cdot CH_3CN$ (2). Naph-ethynyl-terpy (0.025 g, 0.065 mmol) was dissolved in CH_3Cl (20 mL), and $Co(BF_4)_2\cdot 6H_2O$ (0.041 g, 0.12 mmol) dissolved in MeOH (15 mL) was added to the solution. The colour immediately changed to brown, and the solution was stirred for 3 h. The solution was concentrated, and the resulting precipitate was filtered to obtain a crude brown powder. Single crystals of **2** were obtained by inducing the diffusion of ether into a CH_3CN solution of the crude brown powder. Yield: 62%. Elemental analysis (%): calcd. for $C_{58}H_{40}B_2CoF_8N_8$: calcd., C, 64.41; H, 3.73; N, 10.36. Found: C, 64.03; H, 3.85; N, 10.52. ESI-MS: calculated $m/z = 412.9106$, observed $m/z = 412.3211$.

2.1.5 Synthesis of $[Co(Ant\text{-}ethynyl\text{-}terpy)_2](BF_4)_2$ (3). Ant-ethynyl-terpy (0.084 g, 0.022 mmol) was dissolved in $CH1_3Cl$ (20 mL), and $Co(BF_4)_2\cdot 6H_2O$ (0.045 g, 0.11 mmol) dissolved in MeOH (15 mL) was added to the solution. The colour immediately changed to brown, and the solution was stirred for 3 h. The solution was concentrated, and the resulting precipitate was filtered to recover the crude product as a brown powder. Single crystals of **3** were grown by inducing the diffusion of ether into a CH_3CN solution of the crude brown powder. Yield: 55%. Elemental analysis (%): calcd. for $[Co(Ant\text{-}ethynyl\text{-}terpy)_2](BF_4)_2\cdot 3.5H_2O$ ($C_{62}H_{45}B_2CoF_8O_{3.5}$): calcd., C, 64.05; H, 3.90; N, 7.23. Found: C, 64.22; H4.16; N, 6.92. ESI-MS: calculated $m/z = 462.9692$, observed $m/z = 462.6261$.

2.1.6 Synthesis of $[Co(Pyr\text{-}ethynyl\text{-}terpy)_2](BF_4)_2\cdot 3CHCl_3$ (4). Pyr-ethynyl-terpy (0.084 g, 0.022 mmol) was dissolved in CH_3Cl (20 mL), and $Co(BF_4)_2\cdot 6H_2O$ (0.045 g, 0.11 mmol) dissolved in MeOH (15 mL) was added to this solution. The colour immediately changed to brown, and the solution was filtered. The filtrate was allowed to stand for 1 week to dark reddish-brown crystals of **4**. Yield: 58%. Elemental analysis (%): calcd for $C_{68.7}H_{42.7}B_2Cl_{8.1}CoF_8N_6$: calcd., C, 56.06; H, 2.92; N, 5.71. Found: C, 56.16; H, 3.20; N, 5.75. ESI-MS: calculated $m/z = 486.6245$, observed $m/z = 487.6263$t.

2.2 Physical measurements

^{1}H NMR and ^{13}C NMR spectra were recorded on a spectrometer (JEOL 500-ECX) by using a deuterated solvent as the lock and

a residual solvent (or tetramethylsilane) as the internal reference. Elemental analyses (C, H, and N) were carried out on a J SCIENCE LAB JM10 analyser at the Instrumental Analysis Centre at Kumamoto University, Japan. The structure of **1** or **2–4** was determined by single-crystal X-ray diffraction (XRD) analysis at 100 K using a Rigaku Saturn724 diffractometer or Rigaku XtaLAB mini II diffractometer equipped with a confocal mirror using graphite-monochromated Mo Kα radiation ($\lambda = 0.71075$ Å or 0.71073 Å). The data were integrated and reduced using CrysAlisPro software. The crystal structures were solved with the ShelXT structure solution program in Olex2 using direct methods and refined by full-matrix least-squares refinement using the ShelXL program. Hydrogen atoms were geometrically refined using a riding model. Temperature-dependent magnetic susceptibilities were measured on a superconducting quantum interference device magnetometer (Quantum Design MPMS XL). For these measurements, the crystalline samples were placed in a capsule mounted inside a straw. Ultraviolet-visible (UV-vis) and fluorescence spectra were recorded using a Shimadzu UV-3600 spectrophotometer and a PerkinElmer LS55 spectrofluorometer, respectively. A 20 μM solution of each complex was prepared in acetonitrile for the UV-vis spectral measurements. In addition, 20 μM and 100 μM solutions of each complex were prepared in acetonitrile for measuring the fluorescence spectra. ESI-TOF MS was measured using Xevo G2-XS QTof in acetonitrile.

3 Results and discussion

3.1 Crystal structures

Four Co(II) compounds $[Co(R\text{-ethynyl-terpy})_2](BF_4)_2$ were synthesised *via* ether diffusion or slow evaporation. The single-crystal structures of complexes **1–4** were determined by X-ray crystallography at 100 K; the corresponding crystallographic data and selected bond lengths are presented in Tables S1 and S2.

Complex **1** crystallises in the monoclinic *Cc* space group, and its cation unit is illustrated in Fig. S1. Two crystallographically unique complex cations, *viz.*, Co1 and Co2, are present, which are octahedrally coordinated to two tridentate meridional terpyridine-derivative ligands (ph-ethyl-terpy) with one lattice water molecule and two BF_4^- counter anions, respectively. The corresponding Co–N distances are Co–N1 = 2.054(5) Å, Co–N2 = 1.878(5) Å, Co–N3 = 2.054(5) Å, Co–N4 = 2.106(6) Å, Co–N5 = 1.903(5) Å, Co–N6 = 2.095(5) Å at the Co1 site, and Co–N7 = 2.066(6) Å, Co–N8 = 1.884(5) Å, Co–N9 = 2.065(5) Å, Co–N10 = 2.100(4) Å, Co–N11 = 1.910(5) Å, and Co–N12 = 2.102(5) Å at the Co2 site. Table S2 presents selected bond lengths for complex **1** and the other complexes. The bond lengths in complex **1** are consistent with those of typical LS Co(II) compounds.[20] The distortion parameters Σ for the $[CoN_6]$ core were calculated where Σ is the sum of $|90-\alpha|$ for the 12 *cis*-N–Co–N angles. Σ for **1** are 85.70° and 86.00°, which are also indicative of typical LS

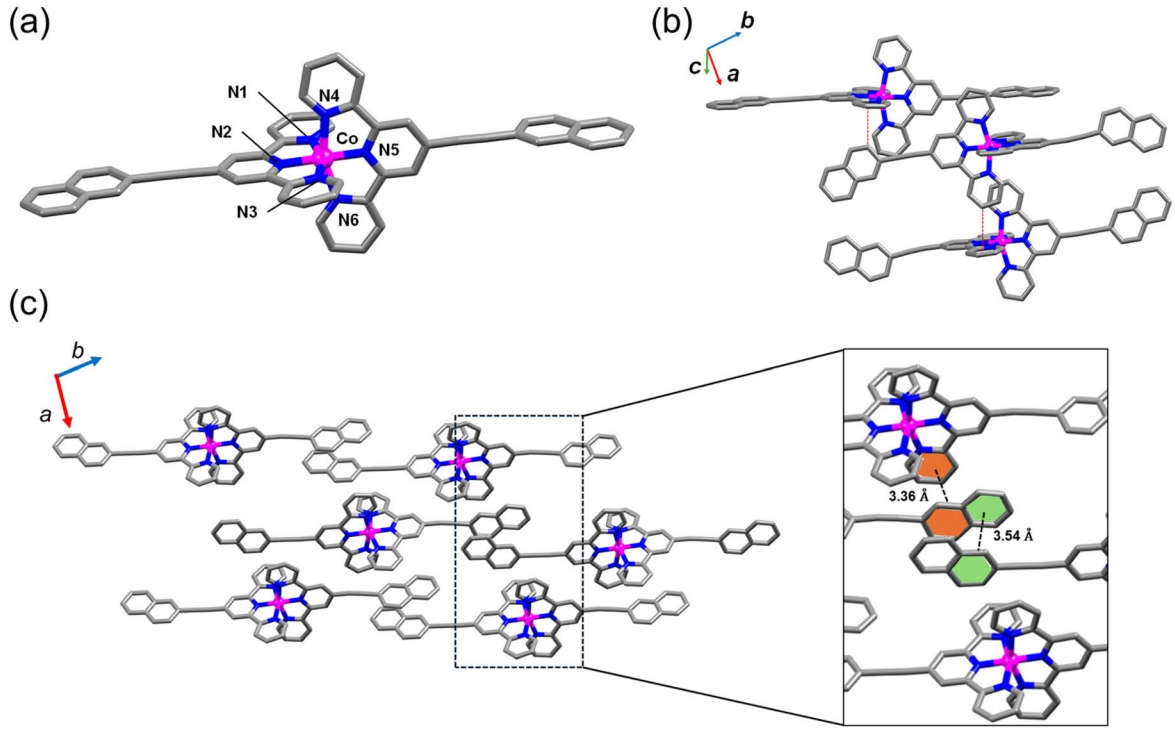

Fig. 1 (a) Molecular structure of **2**. Hydrogen atoms, counter anions and solvent molecules are omitted for clarity. Colour code: Co—magenta, C—grey, N—blue. (b) and (c) packing structure of **2**. Pyridine rings in terpyridine ligand contact with naphthalene rings *via* π–π stacking (3.36 Å) and CH–π interaction (2.77 Å). The terpyridine ligands also exhibit CH–π interactions (2.85 Å) with each other, and the naphthalene rings show π–π stacking (3.54 Å) with each other.

Co(II) complexes.[22] The two ph-ethynyl-terpy moieties in $1 \cdot H_2O$ engage in CH−π interactions between neighbouring complex cations (with a C(43)–H(43) hydrogen to ring-centroid distance of 2.831 Å) (Fig. S1b).

Complex **2** crystallises in the monoclinic $P2_1/c$ space group, and its cationic moiety is nearly identical to that of **1** (Fig. 1). Complex **2** contains one crystallographically unique complex cationic unit of Co1. The corresponding Co–N distances are Co–N1 = 2.044(2) Å, Co–N2 = 1.880(1) Å, Co–N3 = 2.051(2) Å, Co–N4 = 2.103(2) Å, Co–N5 = 1.901(1) Å, and Co–N6 = 2.094(1) Å. The bond lengths are consistent with those of typical LS Co(II) compounds.[20] Selected bond lengths for complex **2** are summarised in Table S2. The calculated distortion parameter Σ for **2** is 85.11°, which is consistent with that of typical LS Co(II) complexes.[22] Each acetonitrile molecule in the crystal packing structure forms hydrogen bonds with the terpy units and ethynyl groups. The BF_4^- ions form hydrogen bonds with the terpy units. The two naphthalene groups in the terpy-derivative ligands in **2** assemble through π–π (naphthalene ring-centroid distance of 3.54 Å) interactions with their adjacent cores oriented along the *ab* direction; the $[Co(terpy\text{-}X)_2]^{2+}$ cation units are layered in the *ab* plane with infinite π–π stacking interactions (Fig. 1b and c).

Complex **3**, containing one crystallographically unique complex cationic unit of Co1, crystallises in the monoclinic $P2_1/c$ space group (Fig. S2). The corresponding Co–N distances are Co–N1 = 2.104(3) Å, Co–N2 = 1.895(3) Å, Co–N3 = 2.120(3) Å, Co–N4 = 2.014(3) Å, Co–N5 = 1.864(3) Å, and Co–N6 = 2.012(3) Å. The bond lengths are consistent with those of typical LS Co(II) compounds,[20] and selected bond lengths for complex **3** are summarised in Table S2. The distortion parameter Σ for **3** is 94.00°, which is consistent with that of typical LS Co(II) complexes.[22] Each acetonitrile molecule in the crystal packing structure forms hydrogen bonds with the terpy units and BF_4^- anions. The BF_4^- ions form hydrogen bonds with the terpy units, whereas the two anthracene groups in the terpy-derived ligands in **3** assemble through π–π (anthracene ring-centroid distance of 3.36 Å) interactions with their adjacent cores oriented along the *ac* direction (Fig. S2).

Complex **4** crystallises in the triclinic $P\bar{1}$ space group and contains one crystallographically unique complex cationic unit of Co1 (Fig. 2). The corresponding Co–N distances are Co–N1 = 2.097(2) Å, Co–N2 = 2.011(2) Å, Co–N3 = 2.095(2) Å, Co–N4 = 2.164(2) Å, Co–N5 = 2.027(3) Å, and Co–N6 = 2.160(2) Å. The bond lengths are consistent with those of typical HS Co(II) compounds.[20] Selected bond lengths for complex **4** are summarised in Table S2. The distortion parameter Σ for **4** (120.69°) is consistent with that of typical HS Co(II) complexes.[22] Each chloroform molecule in the crystal packing structure forms hydrogen and halogen bonds with the BF_4^- ions and hydrogen atoms in the pyrene group, respectively. The BF_4^- ions undergo intermolecular interactions with the terpy units and pyrene groups as well.

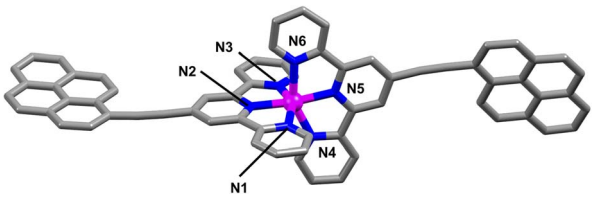

Fig. 2 Molecular structure of **4**. Counter anions, H atoms, and solvent molecules are omitted for clarity. Colour code: Co—magenta, C—grey, N—blue.

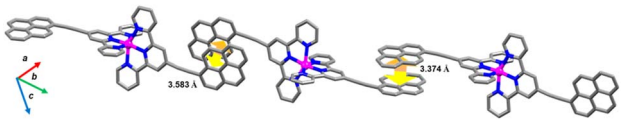

Fig. 3 Packing structure of **4**. Counter anions, H atoms, and solvent molecules are omitted for clarity. Colour code: Co—magenta, C—grey, N—blue.

Complex **4** possesses a characteristic packing structural motif that is attributed to the strong intermolecular interactions between the neighbouring pyrenyl groups at position "4" of the terpyridine ligands. This directional intermolecular π–π packing interaction yields one-dimensional chain structures (the distance between pyrene and pyrene: 3.431 Å, 3.374 Å) (Fig. 3).

3.2 Magnetic properties

The measured temperature-dependent magnetic susceptibilities ($\chi_m = M_m/H$; χ_m: magnetic susceptibility; M_m: magnetisation; H: magnetic field) of complexes **1–4** are plotted in Fig. 4.

The measured magnetic susceptibility values indicate that complexes **1** and **3** display similar, incomplete SCO behaviour owing to their high $T_{1/2}$ values (Fig. 4a and c).[28–33] The $\chi_m T$ values for **1** and **3** are 0.39 and 0.35 $cm^3\ K\ mol^{-1}$ at 5 K, which is

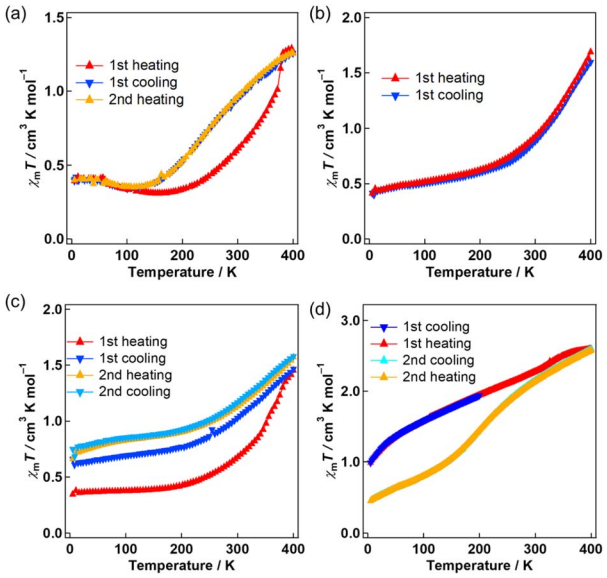

Fig. 4 $\chi_m T$ *vs.* T plots of (a) **1**, (b) **2**, (c) **3**, and (d) **4** in the heating and cooling process in the range of 2–400 K. χ_m: magnetic susceptibility. The mismatch of profiles is owing to the desolvation of samples.

in the range expected for a low-spin cobalt(II) complex ($S = 1/2$). On raising the temperature from 5 K to 400 K, $\chi_m T$ values increased to 1.26 and 1.45 cm^3 K mol^{-1} at 400 K for **1** and **3**. These $\chi_m T$ values are slightly lower than those of previously reported high-spin Co(II) complexes ($S = 3/2$), which is due to the incomplete SCO behaviour in the measured temperature range. The profiles of the samples annealed at 400 K do not align with those of the unheated samples. This result demonstrates that the desolvated **1** and **3** samples exhibit irreversibly changed magnetic profiles due to structural changes induced by the removal of the solvent. Unfortunately, the single-crystal XRD analyses for the desolvated samples did not succeed because of their low-quality single crystals. Therefore, these structural changes after desolvation were confirmed by the powder XRD (PXRD) experiments. Furthermore, the sample decomposition temperatures are higher for complexes **1–4** than 400 K, indicating that these magnetic profile changes are not due to the sample decomposition. This behaviour, in which the magnetic profiles are different between solvated and desolvated samples, is often associated with complexes that are responsive to external stimuli.[34–37] In contrast, complex **2** exhibits reversible SCO behaviour even after heating to 400 K (Fig. 4b), possibly owing to its stable framework structure and coordination environments being maintained by intermolecular interactions during desolvation.

The $\chi_m T$ value of **4** is 1.58 cm^3 K mol^{-1} at 100 K, which is consistent with intermediate values for the LS and HS states of the Co(II) ion (Fig. 4d). This is consistent with the structural data. Upon cooling the temperatures from 100 K to 5 K, the $\chi_m T$ value for **4** gradually decreased from 1.58 at 100 K to 0.99 cm^3 K mol^{-1} at 5 K, which represents incomplete SCO behavior for Co(II) in an octahedral environment and reflects the highly distorted structure present at low temperature. Upon heating the sample, the gradual increase in the $\chi_m T$ value to 2.59 cm^3 K mol^{-1} up to 400 K can be attributed to the SCO behaviour of Co(II) ions. Additionally, the slight differences in the magnetic profile of compound **4** after heating to 400 K reflect the removal of solvent molecules. The second cooling and heating profiles are overlapped, and the $\chi_m T$ value of **4** is 0.80 cm^3 K mol^{-1} at 100 K, which desolvated samples exhibited gradual and complete SCO behavior. These findings are typical for complexes that are responsive to external stimuli.[34–37] Also, there is no characteristic thermal hysteresis during the heating/cooling processes for desolvated samples of complexes **1–4**.[38]

3.3 Photophysical properties

Fig. 5 presents the UV-vis spectra of complexes **1–4** recorded at 300 K in CH_3CN solution. Evidently, these complexes exhibit similar absorption bands in the wavelength ranges 287–391 and 449–534 nm, which are assigned to ligand-centred (LC) π–π* transitions and metal-to-ligand charge transfer, respectively.[39–43] The observation of metal-to-ligand charge transfer bands supports the formation of complexes cation in the acetonitrile solution, as well as the ESI-MS spectroscopy.

Fig. 6a displays the fluorescence spectra of **1–4** measured at 300 K in CH_3CN solution (20 μM) using the excitation

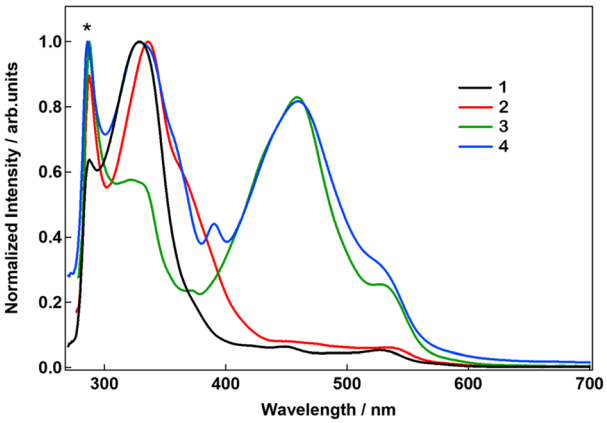

Fig. 5 UV-vis spectra for **1–4** (20 μM) in CH_3CN. The peak marked with a * originates from the device.

wavelengths corresponding to the π–π* transition bands of these complexes. Complexes **1** and **2** exhibit peaks at 419 and 491 nm, respectively, which are assigned to LC π–π* transitions. Complexes **3** and **4** exhibit characteristic luminescence (Fig. 6b) in the form of two (or three) peaks in the wavelength range of 417–650 nm. The peaks at 450–525 and 540–650 nm are

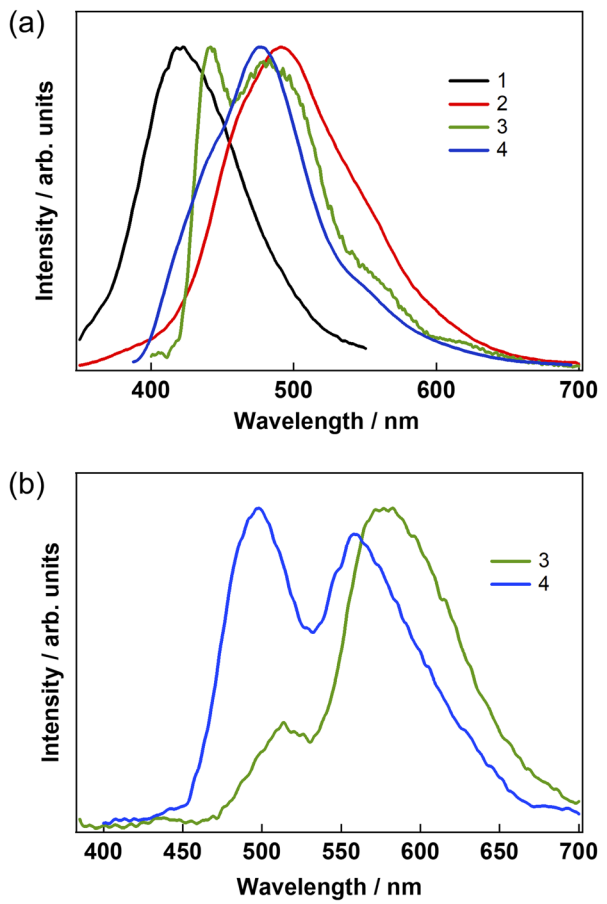

Fig. 6 Fluorescence spectra of (a) **1–4** (20 μM) and (b) **3** and **4** (100 μM) in CH_3CN. The fluorescence spectra were recorded using 317 nm (**1**), 336 nm (**2**), 372 nm (**3**), and 391 nm (**4**) excitation.

attributed to LC π–π* transitions and excimer fluorescence from the anthracene (or pyrene) moieties, respectively. The intensity of excimer fluorescence typically increases with increasing concentration, and the peaks occur at higher wavenumbers than those of monomer fluorescence. Therefore, we additionally recorded the fluorescence spectra of all the compounds in 100 μM CH_3CN solutions (Fig. 6b, S3, and S4). All the compounds underwent fluorescence quenching in the 100 μM CH_3CN solution, whereas no quenching was evident in the 20 μM solution.[44] However, at higher concentrations, **3** and **4** exhibited fluorescence at wavelengths (582 and 565 nm) longer than 450–530 nm (Fig. 6b). Furthermore, **3** and **4** exhibited shoulder peak at around 525–625 or 525–560 nm in the low concentration (20 μM), but the monomer peak intensity is strong. However, the peak intensity at longer wavelength become stronger in the high concentration (100 μM), indicative of the observation of the excimer emission. Therefore, **3** and **4** exhibited excimer fluorescence at 582 or 560 nm, as characteristic of the formation of excimer.

4 Conclusions

In this study, we designed and synthesised a series of $[Co(R\text{-ethynyl-terpy})_2](BF_4)_2$ (R = phenyl, naphthyl, anthracenyl, and pyrenyl) compounds and determined their single-crystal structures and packing arrangements. An examination of their switchable magnetic properties *via* temperature-dependent magnetic susceptibility measurements revealed the SCO behaviour of complexes **1–4**. However, reversible SCO behaviour was only found for complex **2**. Owing to the presence of anthracene and pyrene groups (derived from the ethynyl groups) in the terpyridine units, complexes **3** and **4** exhibited excimer luminescence in CH_3CN solution. The occurrence of spin crossover (SCO) is strongly dependent on, amongst other properties, the transition metal center, coordinating ligands, and coordination geometry of a coordination complex. This study suggests the possibility of synthesizing magnetically functional coordination metal compounds based on Co(II) ions with the potential for developing photophysical materials.

Author contributions

K. Soejima: investigation, formal analysis, data curation; Y. Sekine: conceptualisation, supervision, writing – original draft; K. Miyake, K. Kiba, Y. Yamaguchi, H. Zenno; data curation; S. Hayami: conceptualisation, supervision, project administration, writing – review & editing.

Conflicts of interest

There are no conflicts to declare.

Data availability

The data supporting this article have been included as part of the SI. Supplementary information is available. See DOI: **https://doi.org/10.1039/d4ra08657k**.

Acknowledgements

This work was supported by KAKENHI Grants-in-Aid for Scientific Research JP24K01502 and JP24K08449. This work was also supported by a Ministry of Education, Culture, Sports, Science, and Technology Leading Initiative for Excellent Young Researchers grant (No. JPMXS0320200363) and the Young Faculty Members Support Program of the International Research Organization for Advanced Science and Technology, Kumamoto University, Kumamoto, Japan. Y.S. expresses gratitude to the Iketani Science and Technology Foundation. The authors thank Ms. Emi Kubota for her help with the synthesis of the complexes.

References

1 O. Sato, *Nat. Chem.*, 2016, **8**, 644.
2 M. E. Guillermo and E. Coronado, *Chem. Soc. Rev.*, 2018, **47**, 533.
3 A. Dei, D. Gatteschi, C. Sangregorio and L. Sorace, *Acc. Chem. Res.*, 2004, **37**, 827.
4 E. Coronado, *Nat. Rev. Mater.*, 2019, **5**, 87.
5 K. S. Kumar and M. Ruben, *Angew. Chem., Int. Ed.*, 2021, **60**, 7502.
6 K. S. Kumar and M. Ruben, *Coord. Chem. Rev.*, 2017, **346**, 176.
7 G. Molnár, S. Rat, L. W. Nicolazzi and A. Bousseksou, *Adv. Mater.*, 2017, **30**, 1703862.
8 P. Gütlich, Y. Garcia and H. A. Goodwin, *Chem. Soc. Rev.*, 2000, **29**, 419.
9 P. Gütlich and H. A. Goodwin, *Spin Crossover in Transition Metal Compounds*, Springer Science & Business Media, vol. 233–235, 2004.
10 H. A. Goodwin, *Spin Crossover in Transition Metal Compounds II*, Springer, Berlin, Heidelberg, 2004, pp. 23–47.
11 J. S. Miller and K. S. Min, *Angew. Chem., Int. Ed.*, 2009, **48**, 262.
12 M. Mitsumi, T. Nishitani, S. Yamasaki, N. Shimada, Y. Komatsu, K. Toriumi, Y. Kitagawa, M. Okumura, Y. Miyazaki, N. Córska, A. Inaba, A. Kanda and N. Hanasaki, *J. Am. Chem. Soc.*, 2014, **136**, 7026.
13 M. Nihei, Y. Sekine, N. Suganami, K. Nakazawa, A. Nakano, H. Nakano, Y. Murakami and H. Oshio, *J. Am. Chem. Soc.*, 2011, **133**, 3592.
14 D. F. Li, R. Clérac, O. Roubeau, E. Harté, C. Mathonière, R. L. Bris and S. M. Holmes, *J. Am. Chem. Soc.*, 2008, **130**, 252.
15 H. Miyasaka, N. Motokawa, T. Chiyo, M. Takemura, M. Yamashita, H. Sagayama and T. Arima, *J. Am. Chem. Soc.*, 2011, **133**, 5338.
16 J. Chen, Y. Sekine, Y. Komatsumaru, S. Hayami and H. Miyasaka, *Angew. Chem., Int. Ed.*, 2018, **57**, 12043.
17 J. Chen, Y. Sekine, A. Okazawa, H. Sato, W. Kosaka and H. Miyasaka, *Chem. Sci.*, 2020, **11**, 3610.
18 Y. Sekine, J. Chen, N. Eguchi and H. Miyasaka, *Chem. Commun.*, 2020, **56**, 10867–10870.
19 R. Fukushima, Y. Sekine, Z. Zhang and S. Hayami, *J. Am. Chem. Soc.*, 2024, **146**(35), 24238.

20 (*a*) S. Hayami, Y. Komatsu, T. Shimizu, H. Kamihata and Y. H. Lee, *Coord. Chem. Rev.*, 2011, **255**, 1981–1990; (*b*) P. Nielsen, H. Toftlund, A. D. Bond, J. F. Boas, J. R. Pilbrow, G. R. Hanson, C. Noble, M. J. Riley, S. M. Neville, B. Moubaraki and K. S. Murray, *Inorg. Chem.*, 2009, **48**, 7033; (*c*) R. Nakahara, M. Nakaya, J. W. Shin, R. Ohtani, M. Nakamura, Y. Zhang, L. F. Lindoy and S. Hayami, *Aust. J. Chem.*, 2017, **70**, 494–498, DOI: **10.1071/CH16556**; (*d*) N. Izumiyama, S. Fujii, K. Kato, R. Tokunaga, S. Hayami and M. Nakaya, *Dalton Trans.*, 2024, **53**, 9547.

21 S. Hayami, Y. Shigeyoshi, M. Akita, K. Inoue, K. Kato, K. Osaka, M. Takata, R. Kawajiri, T. Mitani and Y. Maeda, *Angew. Chem., Int. Ed.*, 2005, **44**, 4899.

22 M. Nakaya, R. Ohtani, J. W. Shin, M. Nakamura, L. F. Lindoy and S. Hayami, *Dalton Trans.*, 2018, **47**, 13809–13814.

23 R. Akiyoshi, Y. Komatsumaru, M. Donoshita, S. Dekura, Y. Yoshida, H. Kitagawa, Y. Kitagawa, L. F. Lindoy and S. Hayami, *Angew. Chem., Int. Ed.*, 2021, **60**, 12717–12722.

24 S. Ott, M. Borgström, M. Kritikos, R. Lomoth, J. Bergquist, B. Akermark, L. Hammarström and L. Sun, *Inorg. Chem.*, 2004, **43**, 4683–4692.

25 S. Hachiya, K. Asai and G. Konishi, *Tetrahedron Lett.*, 2013, **54**, 1839–1841.

26 T. Zdobinsky, P. S. Maiti and R. Klajn, *J. Am. Chem. Soc.*, 2014, **136**, 2711–2714.

27 M. Hissler, A. Harriman, A. Khatyr and R. Ziessel, *Chem.–Eur. J.*, 1999, **5**, 3366.

28 P. Guionneau, M. Marchivie, G. Bravic, J. F. Léetard and D. Chasseau, *J. Mater. Chem.*, 2002, **12**, 2546.

29 J. Zarembowitch and O. Kahn, *Inorg. Chem.*, 1984, **23**, 589.

30 Y.-C. Sun, F.-L. Chen, K.-J. Wang, Y. Zhao, H.-Y. Wei and X.-Y. Wang, *Inorg. Chem.*, 2023, **62**, 14863.

31 H. Zenno, Y. Sekine, Z. Zhang and S. Hayami, *Dalton Trans.*, 2024, **53**, 5861.

32 D. Schweinfurth, S. Demeshko, S. Hohloch, M. Steinmetz, J. G. Brandenburg, S. Dechert, F. Meyer, S. Grimme and B. Sarkar, *Inorg. Chem.*, 2014, **53**(16), 8203.

33 I. Krivokapic, M. Zerara, M. L. Daku, A. Vargas, C. Enachescu, C. Ambrus, P. Tregenna-Piggott, N. Amstutz, E. Krausz and A. Hauser, *Coord. Chem. Rev.*, 2007, **251**, 364.

34 Y. Sekine, M. Nihei and H. Oshio, *Chem. Lett.*, 2014, **43**, 1029.

35 K. Mitsumoto, E. Oshiro, H. Nishikawa, T. Shiga, Y. Yamamura, K. Saito and H. Oshio, *Chemistry*, 2011, **17**, 9612–9618, DOI: **10.1002/chem.201101404**.

36 S. De, J. R. Jiménez, Y. Li, L. M. Chamoreau, A. Flambard, Y. Journaux, A. Bousseksou and R. Lescouëzec, *RSC Adv.*, 2016, **6**, 17456.

37 L. Cao, J. Tao, Q. Gao, T. Liu, Z. Xia and D. Li, *Chem. Commun.*, 2014, **50**, 1665.

38 R. G. Miller, S. Narayanaswamy, J. L. Tallon and S. Brooker, *New J. Chem.*, 2014, **38**, 1135–1146.

39 N. W. Alcock, P. R. Barker, J. M. Haider, M. J. Hannon, C. L. Painting, Z. Pikramenou, E. A. Plummer, K. Rissanen and P. Saarenketo, *J. Chem. Soc., Dalton Trans.*, 2000, 1447–1462.

40 Sonia, A. K. Pandey, I. Verma and B. N. Mongal, *Chem. Phys. Impact*, 2024, **9**, 100706.

41 E. U. Mughal, M. Mirzaei, A. Sadiq, S. Fatima, A. Naseem, N. Naeem, N. Fatima, S. Kausar, A. A. Altaf, M. N. Zafar and B. A. Khan, *R. Soc. Open Sci.*, 2020, **7**, 201208.

42 P. Liu, G. Shi and X. Chen, *Front. Chem.*, 2020, **8**, 592055.

43 C. Enachescu, I. Krivokapic, M. Zerara, J. A. Real, N. Amstutz and A. Hauser, *Inorg. Chim. Acta*, 2007, **360**, 3945.

44 K. D. Chaudhuri, *Z. Phys.*, 1959, **154**, 34–42.